

## Reduced Graphene oxide -coated 3D interconnected SiO<sub>2</sub> Nanoparticles with Enhanced Lithium Storage Performance

Xu Guo, Kai Xie, Yourong Wang\*, Zhengya Kang, Wei Zhou and Siqing Cheng\*

Innovation Center for Nanomaterials in Energy and Medicine (ICNEM), School of Chemical and Environmental Engineering, Wuhan Polytechnic University, Hubei 430023, P. R. China

\*E-mail: [chengsqing@iccas.ac.cn](mailto:chengsqing@iccas.ac.cn)

Received: 15 February 2018 / Accepted: 9 April 2018 / Published: 10 May 2018

---

3D interconnected SiO<sub>2</sub> nanoparticles coated by reduced graphene oxide (rGO) (SiO<sub>2</sub>@rGO) were fabricated easily by online hydrolysis and subsequent condensation of the precursor tetraethylorthosilicate (TEOS) in the dispersed graphene oxide (GO) sol, followed by the reduction of GO using hydrazine hydrate. The as-obtained 3D interconnected SiO<sub>2</sub> nanoparticles coated by rGO composites as anode material for lithium ion rechargeable batteries (LIBs) delivers a reversible discharge capacity of 490.7 mAh g<sup>-1</sup> at a current density of 100 mA g<sup>-1</sup> after 60 cycles with the coulombic efficiency of nearly 98%. Compared to the bare nano-SiO<sub>2</sub>, the enhanced lithium storage performance could be attributed to its unique 3D interconnected network space structure to accommodate the volume variation during cycled lithiation/delithiation process.

---

**Keywords:** SiO<sub>2</sub>; Sol-gel method; Anode materials; Lithium ion batteries.

### 1. INTRODUCTION

Si-based materials have been recognized as the most promising anode candidate for the next generation lithium ion rechargeable batteries (LIBs) with high energy and powder density in terms of their highest theoretical capacity of 4200 mAh g<sup>-1</sup> corresponding to the product Li<sub>22</sub>Si<sub>5</sub> and low stable plateau operation voltage of ~ 0.4 V versus Li/Li<sup>+</sup>[1-3]. Unfortunately, the huge volume variation during repeated charge/discharge process results in the rapid pulverization of the relative material and thus remarkable capacity decay [4–6]. Thus, some investigations have been made to create the unique structured Si-based composites in order to ameliorate the cycling performance of Si anode [4,7–10]. Nonetheless, the implementation of practical application is hindered severely owing to the intricate and expensive fabrication processes.

Thus, many researchers have took cognizance of oxide of Si, i.e. SiO<sub>2</sub> with many similar superiorities to that of Si, such as high theoretical specific capacity of 1961 mAh g<sup>-1</sup> and low discharge

potential, but other than that it is low cost available material anywhere [1,11–13]. More importantly, in comparison with silicon, SiO<sub>2</sub> shows less volume variation during repeated charge/discharge process. According to the lithiation/delithiation mechanism of SiO<sub>2</sub> as anode material, the generated nano-Si is embedded uniformly in the generated inert matrix containing lithium oxide (Li<sub>2</sub>O)/lithium silicates (Li<sub>4</sub>SiO<sub>4</sub>) once SiO<sub>2</sub> is lithiated initially, thus the individual nano-Si would generate only weak volume variation during the following lithiation, which is also prevented by the stress of the generated inert matrix and thus make geometrically the electrode integrity. As such, the volume variation during the whole process is accommodated. [14–17] However, it should be noted that the pure SiO<sub>2</sub> was suitable for electrode materials due to its electrochemical inertness and strong Si-O bond although Gao et al. [18] found that commercial SiO<sub>2</sub> nanoparticles could react with lithium ion in the certain voltage range. Besides, there still exist a certain inner stress of SiO<sub>2</sub> due to the volume variation upon Li insertion/extraction process of SiO<sub>2</sub>, which must also be considered when fabricating the new SiO<sub>2</sub> electrode [19–22]. In order to circumvent these issues, many strategies have been proposed to improve the electrochemical performance of SiO<sub>2</sub> electrode by fabricating SiO<sub>2</sub> nanoparticles [23,24], hollow porous nano-SiO<sub>2</sub> [14,25], SiO<sub>2</sub> thin films [21], SiO<sub>2</sub>-based nanocomposites [11] et al. It has been widely recognized that coating SiO<sub>2</sub> with carbonaceous materials including active carbon (carbon black), carbon nanotubes, carbon fibers, graphene and so on [1,26–31] is a feasible and effective strategy to enhance the conductivity of SiO<sub>2</sub> and accommodate its volume expansion during lithium insertion/extraction. In recent years, graphene as a novel and highly conductive nanocarbon component has been successfully applied as various electrode materials due to its high specific surface area of over 2630 m<sup>2</sup> g<sup>-1</sup>, outstanding conductivity of 2.5×10<sup>5</sup> cm<sup>2</sup>V<sup>-1</sup>s<sup>-1</sup>, superior structural flexibility and mechanical strength [29,30], exhibiting a remarkable potential in boosting the electrochemical activeness of the electrode materials. However, graphene is not produced easily and costs a lot, which might impede the practical application of implementation. Herein, we made an attempt to replace graphene by its derivative, reduced graphene oxide (rGO) which is facile and scalable production, to coat SiO<sub>2</sub> to generate the 3D space network architecture so that it could enhance the electronic conductivity of SiO<sub>2</sub> and buffer the volume variation during the repeated charge/discharge process although some reports have showed SiO<sub>2</sub>@rGO composites as anode for LIBs with no better results than that of SiO<sub>2</sub>@GO [32,33]. The results show a facile method of preparing SiO<sub>2</sub>@rGO nanocomposites and the excellent electrochemical performance of the as-prepared 3D interconnected network SiO<sub>2</sub>@rGO nanocomposites as anode, indicating the role of the unique architecture in alleviating the electrochemical performance of SiO<sub>2</sub> as electrode materials.

## 2. EXPERIMENTAL SECTION

### 2.1. Materials and synthesis

All of the chemicals in this work were purchased from Sinopharm Chemical Reagent Co., Ltd., Shanghai and used without further purification unless otherwise stated. The nano-SiO<sub>2</sub> was prepared in accordance with our previous work [32]. Briefly, 5 ml of tetraethylorthosilicate (TEOS) was added dropwise into 170 ml of ethanol solution containing 2 ml of 20% NH<sub>3</sub>·H<sub>2</sub>O solution under stirring. After reacted for 24 h, the generated silica was collected by centrifugation and washed with absolute

ethanol for 5 times, and then dried at 100 °C overnight. Finally, the as-obtained nano-SiO<sub>2</sub> is calcined in a muffle furnace at 600 °C for 6 h. Graphene oxide (GO) was synthesized from graphite flakes by a modified Hummers' method.[34,35] In a typical procedure, 40 ml of 98% H<sub>2</sub>SO<sub>4</sub> was slowly added dropwise into the mixture containing 0.6 g of graphite flakes and 0.4 g of NaNO<sub>3</sub> in an water bath environment under vigorous stirring. After reaction for 3 h, 2 g of KMnO<sub>4</sub> were added step by step under stirring. The resultant mixture was subjected to react for six days at room temperature. Afterwards, 50 ml of 10 wt% H<sub>2</sub>SO<sub>4</sub> aqueous solution was added gradually over about 5 h under stirring. The as-obtained mixture was further reacted for another 5 h. Then, 2 ml of 20 wt% H<sub>2</sub>O<sub>2</sub> aqueous solution was added and stirred for another 2 h. The resultant mixture was centrifuged and washed by ID water and an aqueous solution containing 5 wt% H<sub>2</sub>SO<sub>4</sub> and 1 wt% H<sub>2</sub>O<sub>2</sub> for 6 times to get rid of ions of reactant until the pH of the system was about 6.5. The resultant product was dried under vacuum at 100 °C for 12 h. SiO<sub>2</sub>@rGO nanocomposites was prepared as follows: 0.15 g of the as-prepared GO above was dispersed in the mixed aqueous solution containing 30 ml of deionized water, 160 ml of absolute ethanol and 5 ml of 25% NH<sub>3</sub>·H<sub>2</sub>O solution, 4 ml of TEOS in a 250 ml beaker under stirring. The resultant mixture was further stirred for 12 h at room temperature and then reduced by a certain amount of hydrazine hydrate. The resulting mixture was centrifuged and washed by deionized water and ethanol, respectively for many times. The as-obtained sample was dried under vacuum at 60 °C for 24 h.

## 2.2. Materials characterization

Phase structures of the as-prepared samples were characterized by powder X-ray diffraction (XRD) on a Shimadzu DX-7000 advanced X-ray diffraction operated at 40 kV and 40 mA using Cu K $\alpha$  radiation ( $\lambda = 0.154$  nm) over  $2\theta$  degree from 10° to 70° at a scan rate of 4° min<sup>-1</sup>. The morphology and shape of the as-prepared samples were examined using a Hitachi scanning electron microscopy (SEM) and a JEOL TEM-2010 transmission electron microscopy (TEM) operating at an acceleration voltage of 200 kV. Raman spectroscopy measurements were taken using a micro-Raman system (Renishaw, RM1000-In Via) with excitation energy of 2.41 eV (514 nm). The reduced graphene oxide content was determined by thermogravimetric analysis (TGA) with a heating rate of 10 °C min<sup>-1</sup> operating in air atmosphere. The electrochemical impedance spectroscopy (EIS) measurements were performed in two-electrode cells on a CHI660B electrochemical workstation (Chenghua, Shanghai, China) with a  $\pm 5$  mV AC signal amplitude, and the frequency ranged from 10kHz to 0.1 Hz. Cyclic voltammetry (CV) measurements were carried out over a potential voltage of 0-3 V (vs. Li/Li<sup>+</sup>) at a scan rate of 0.2 mV s<sup>-1</sup>.

## 2.3. Electrochemical measurement

All the electrochemical performance was examined in two-electrode coin CR2016 half-cell consisting of a working electrode, a separator and a negative electrode (metallic lithium foil). To prepared the working electrodes, 60 wt.% active material, 30 wt.% of super P-2000 (carbon black) as a conductive material and 10 wt.% of polyvinylidene fluoride (PVdF) as a binder were dispersed in N-

methylpyrrolidinone (NMP) solvent. Then, the slurry was cast on a copper foil and dried under vacuum at 80 °C for 24 h. The cells were assembled in an Argon-filled Mikrouna lab glovebox with active material as the working electrode, lithium foil was used as the counter electrode. The electrolyte was composed of 1 M LiPF<sub>6</sub> dissolved in the mixture of ethylene carbonate and diethyl carbonate in a 1:1 volume ratio. Charge-discharge characteristics were tested on a LAND battery system in a voltage range of 0-3 V versus Li/Li<sup>+</sup>.

### 3. RESULTS AND DISCUSSION

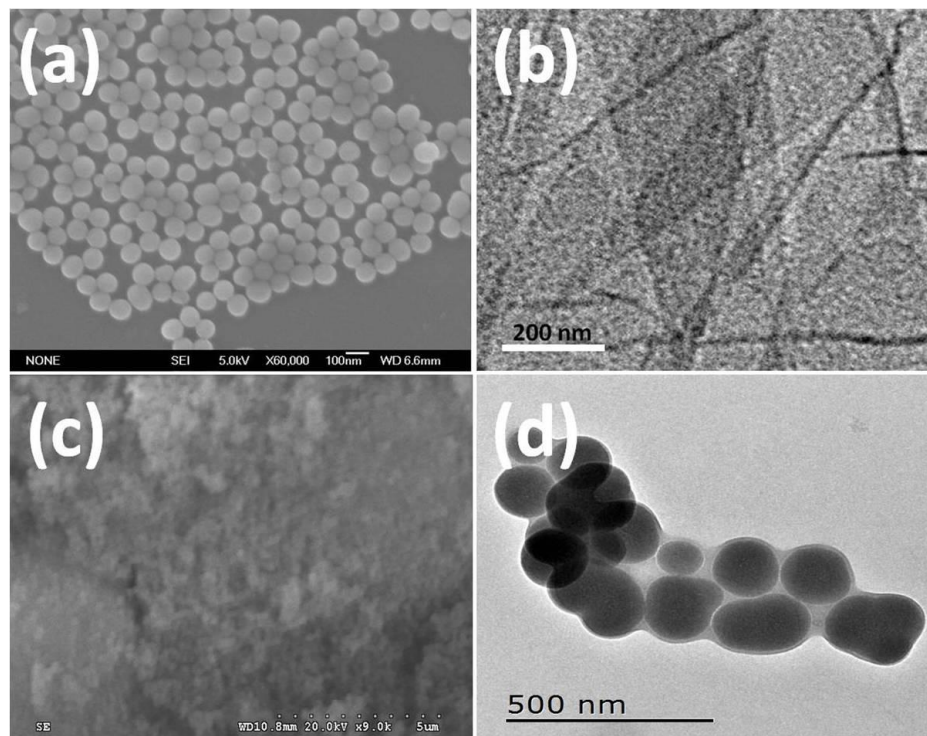


**Figure 1.** (a) SEM image of the as-obtained nano-SiO<sub>2</sub>; (b) TEM image of the as-obtained graphene oxide; (c) SEM image of the as-obtained SiO<sub>2</sub>@rGO; (d) TEM image of the as-obtained SiO<sub>2</sub>@rGO.

The uniformly monodispersed as-made nano-SiO<sub>2</sub> with a size of about 80 nm in diameter by sol-gel method was synthesized by TEOS as the precursor, as shown in Fig. 1a for the SEM image. Fig. 1b shows the TEM image of the as-prepared GO, revealing GO material consisting of randomly aggregated, crumpled sheets closely associated with each other and forming a disordered solid. The SiO<sub>2</sub>@rGO nanocomposites were fabricated by the hydrolysis and condensation of the precursor TEOS of SiO<sub>2</sub> anchored on the surface of the dispersed GO via the electrostatic interaction and subsequent reduction using hydrazine hydrate, as shown in Fig. 1c and 1d for SEM and TEM images. It is seen that rGO is uniformly coated on the surface of SiO<sub>2</sub> to form the thin surface-coated layer although the online grown nano-SiO<sub>2</sub> is not very even with a size below 120 nm in diameter. To further verify the deposited rGO on the surface of nano-SiO<sub>2</sub>, Raman spectra analysis was employed to evaluate the structural features (order/disorder), as illustrated in Fig. 2a for Raman spectra of GO and

SiO<sub>2</sub>@rGO. The D and G bands are appeared around  $\sim 1340\text{ cm}^{-1}$  and  $\sim 1578\text{ cm}^{-1}$ , respectively, and the I<sub>D</sub>/I<sub>G</sub> ratio of SiO<sub>2</sub>@rGO increases notably compared to that of GO, indicating the disorder increase in rGO on the surface of SiO<sub>2</sub> and high quantity of structural defects of rGO [36,37].

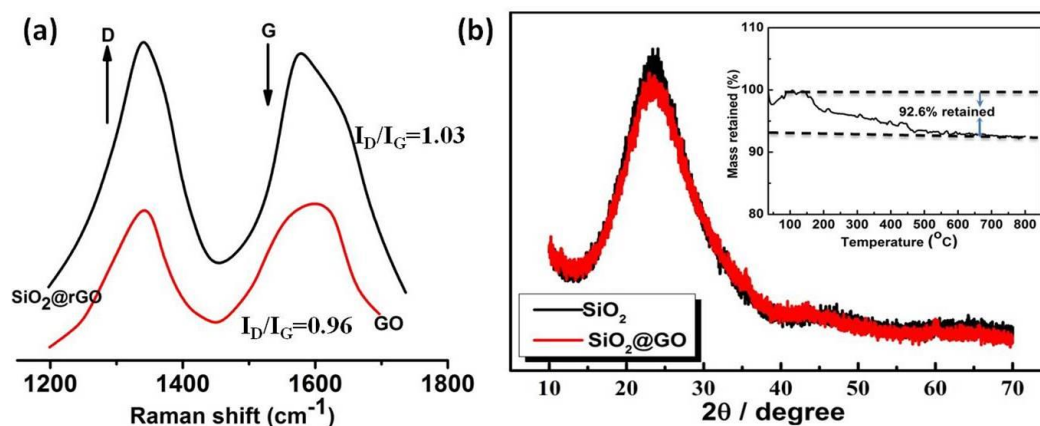


**Figure 2.** (a) Raman spectra of GO (red) and SiO<sub>2</sub>@rGO (black); (b) The X-ray diffraction patterns of SiO<sub>2</sub> and SiO<sub>2</sub>@rGO nanocomposites; Inset: TG curve measured under an air atmosphere of SiO<sub>2</sub>@rGO nanocomposites.

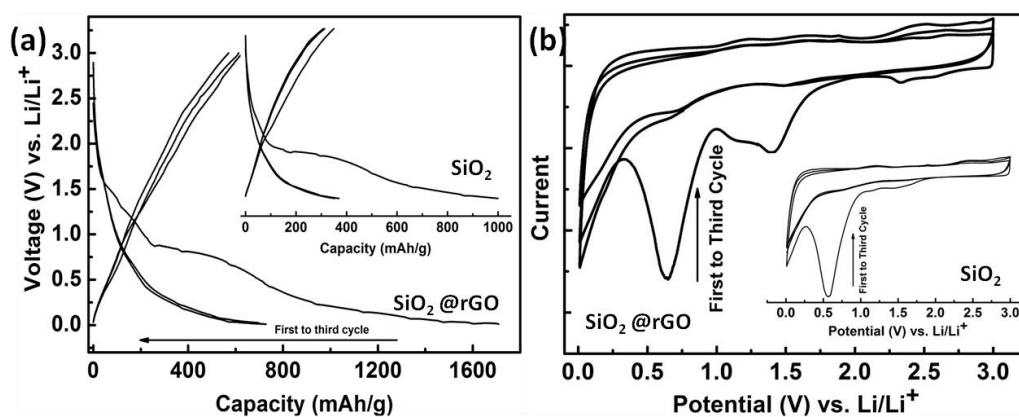


**Figure 3.** (a) The charge-discharge profiles of the as-prepared SiO<sub>2</sub>@rGO nanocomposites for the first three cycles within a voltage of 0-3V versus Li/Li<sup>+</sup>; Inset: the corresponding profiles of the bare nano-SiO<sub>2</sub> for comparison; (b) Cyclic voltammograms of the as-prepared SiO<sub>2</sub>@rGO nanocomposites for the first four cycles from 0 to 3 V versus Li/Li<sup>+</sup> at a scan rate of 0.2 mV s<sup>-1</sup>; Inset: the corresponding cyclic voltammograms of the bare nano-SiO<sub>2</sub> for comparison.

All these can be further confirmed by the powder X-ray diffraction (XRD) patterns of nano-SiO<sub>2</sub> and SiO<sub>2</sub>@rGO nanocomposites, as shown in Fig. 2b. No distinct diffraction peaks are observed but a broad and weak diffraction peak is located in the  $2\theta$  range of 21-23° associated with amorphous SiO<sub>2</sub>, suggesting the amorphous nature of the powders. The coated rGO content in the SiO<sub>2</sub>@rGO nanocomposites is determined to be about 7.4 wt% by thermogravimetric analysis (TGA), as shown in the inset of Fig. 2b, revealing the thin rGO layer on the surface of SiO<sub>2</sub>, which agrees with the results of TEM image.

The electrochemical performances of the as-prepared SiO<sub>2</sub>@rGO nanocomposites were evaluated by assembling two-electrode 2016 coin cells using Li metal counter electrode and the electrolyte 1M LiPF<sub>6</sub> in ethylene carbonate(EC)/dimethyl carbonate (DMC). From Fig.3a for the discharge and charge voltage profiles of the as-prepared SiO<sub>2</sub>@rGO nanocomposites for the first three cycles and the inset of Fig.3a for the bare nano-SiO<sub>2</sub> electrode with the same experimental parameters, it can be seen apparently that the specific capacity of nano-SiO<sub>2</sub> is much smaller than that of SiO<sub>2</sub>@rGO nanocomposites. In the initial discharge cycle for both nano-SiO<sub>2</sub> and SiO<sub>2</sub>@rGO electrodes, there are two gradient plateaus from 1.5 to 0.5 V due to the decomposition of electrolytes, indicating the formation of the solid electrolyte interface (SEI) layer. [14,15] in the following cycling, the corresponding slopes become steep gradually and even the plateaus disappear, revealing that SEI layer occur only in the first cycle. The slope below around 0.5 V is corresponding to the irreversible electrochemical reactions between lithium ion and SiO<sub>2</sub> to form Li<sub>2</sub>O and a series of silicate salts, resulting in an extra irreversible capacity and thus low coulombic efficiency. Afterwards, lithium begins to react with the reduced amorphous silicon for Li-alloying, leading to the reversible capacity for subsequent cycles. All charge voltage profiles seem very steep at potentials of over 1.5 V rather than flat. This might be mainly due to the large polarization of the generated material containing nano-Si and some inert matrix by the first conversion of SiO<sub>2</sub> to impede the kinetics of Li-Si alloying. [28] All these characteristics can further be demonstrated in the cyclic voltammetry, as shown in Fig.3b for the first three cycles within a voltage window of 0-3 V versus Li/Li<sup>+</sup> at a scan rate of 0.2 mV s<sup>-1</sup>. The cathodic peaks account for the plateaus in the discharge curve and the anodic peaks correspond to those in the charge curve. As explained above, the obvious first cathodic peaks are due to the decomposition of electrolyte and thus to the formation of SEI layer. It is worth noting that the curves below 0.5 V for nano-SiO<sub>2</sub> is somewhat different from that for SiO<sub>2</sub>@rGO nanocomposites, which is strongly related to the electrochemical reactions between lithium and SiO<sub>2</sub> or the Si generated by the reduction of SiO<sub>2</sub>. The sharper anodic peaks below 0.5 V for SiO<sub>2</sub>@rGO nanocomposites comparable to nano-SiO<sub>2</sub> manifest that rGO as scaffolding accommodates the volume variation during lithium insertion/extraction of SiO<sub>2</sub>, indicating rGO substantially improves the electrochemical properties of SiO<sub>2</sub>. All these results are summarized and compared in Table 1, in which the electrochemical properties of SiO<sub>2</sub>@GA (grapheme) reported in the literature [30] are included as well. It is indicated that the electrochemical properties of SiO<sub>2</sub>@rGO is superior to those of SiO<sub>2</sub>@GA.

**Table 1.** Comparison of electrochemical performance of nano-SiO<sub>2</sub> and SiO<sub>2</sub>@rGO nanocomposites

Items/cycling Performance	SiO <sub>2</sub> @rGO nanocomposites			Nano-SiO <sub>2</sub>			SiO <sub>2</sub> @GA[30]		
	1 <sup>st</sup>	2 <sup>nd</sup>	3 <sup>rd</sup>	1 <sup>st</sup>	2 <sup>nd</sup>	3 <sup>rd</sup>	1 <sup>st</sup>	2 <sup>nd</sup>	3 <sup>rd</sup>
Discharge capacity /mAh g <sup>-1</sup>	1709	708.6	727.6	999.6	369.7	352.8	1042.7	474.5	450.1
Charge capacity /mAh g <sup>-1</sup>	628.9	570.4	612.5	349.4	313.1	308.6	453.3	445.7	438.5
Coulombic efficiency(%)	36.8	80.5	84.2	35.0	84.7	87.5	43.5	93.9	97.4

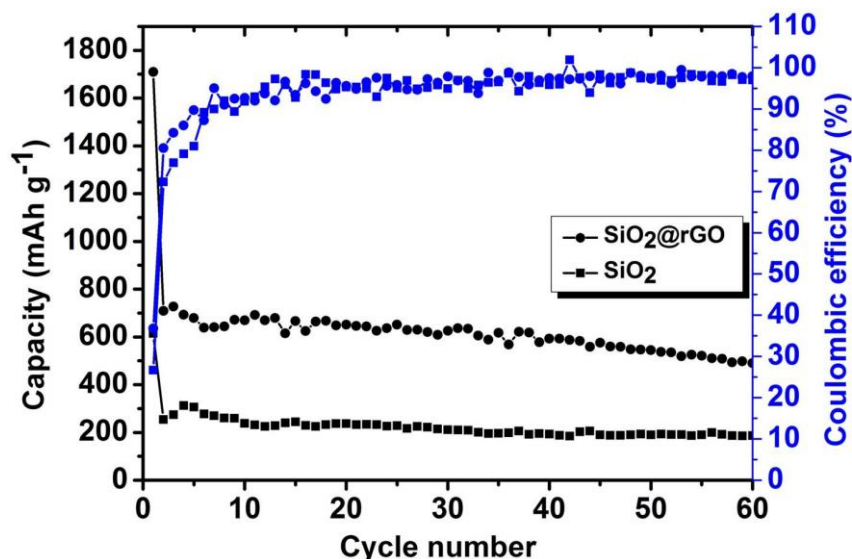


**Figure 4.** Cycling performance and Coulombic efficiency of SiO<sub>2</sub> and SiO<sub>2</sub>@rGO nanocomposites under 100 mA g<sup>-1</sup> within a voltage of 0-3 V versus Li/Li<sup>+</sup>

Fig. 4 shows the cycle performance profiles and the coulombic efficiency of nano-SiO<sub>2</sub>, SiO<sub>2</sub>@rGO nanocomposites at a current density of 100 mA g<sup>-1</sup> for the first 60 cycles. As indicated in the discharge-charge voltage profiles, both nano-SiO<sub>2</sub> and SiO<sub>2</sub>@rGO nanocomposites deliver a high initial discharge capacity and a low initial coulombic efficiency due to the decomposition of the electrolyte and the formation of SEI layer.[14,15] Subsequently, the reversible specific discharge capacity of nano-SiO<sub>2</sub> for the second cycle is only 253.7 mAh g<sup>-1</sup> albeit the discharge capacity still remains 187.3 mAh g<sup>-1</sup> with a capacity retention of 74% after 60 cycles, which is lower than the theoretical capacity (372 mAh g<sup>-1</sup>) of the commercial graphite anode and thus far from the requirement of electrode materials for high-energy lithium ion batteries. Compared with the nano-SiO<sub>2</sub>, the reversible specific discharge capacity of SiO<sub>2</sub>@rGO nanocomposites for the second cycle is 708 mAh g<sup>-1</sup> and after 60 cycles the discharge capacity becomes 490.7 mAh g<sup>-1</sup> with the capacity retention of 69.3% and the coulombic efficiency of 98%, which is much higher than nano-SiO<sub>2</sub> in reversible capacity. As shown in Fig. 5(a), the SiO<sub>2</sub>@rGO nanocomposites also exhibits good cycling rate performance at different current densities. The specific capacity is maintained at values of about 480.6 mAh g<sup>-1</sup> and 396.3 mAh g<sup>-1</sup>, respectively after the current density is increased to 200 mA g<sup>-1</sup> and 300 mA g<sup>-1</sup>, respectively. After the current density is returned to 100 mA g<sup>-1</sup>, the specific capacity is completely restored, exhibiting a good rate capability. All of these results show that the SiO<sub>2</sub>@rGO nanocomposites is indeed a promising strategy to improve the electrochemical performance of SiO<sub>2</sub>.

Such enhanced lithium storage performance of SiO<sub>2</sub>@GO nanocomposites might be attributed to its unique architecture features. Firstly, the shorten path due to the nanoscale of SiO<sub>2</sub> facilitates lithium ion diffusion and electronic transportation in favour of the rate capability. Secondly, the coated rGO sheets on the surface of SiO<sub>2</sub> provides a continuous conductive medium between SiO<sub>2</sub> nanoparticles, thus remarkably enhancing the conductivity of SiO<sub>2</sub>@rGO nanocomposites comparable

to that of nano-SiO<sub>2</sub>, as shown in Fig. 5(b) for the electrochemical impedance spectroscopy (EIS) of nano-SiO<sub>2</sub> and SiO<sub>2</sub>@rGO nanocomposites electrodes.

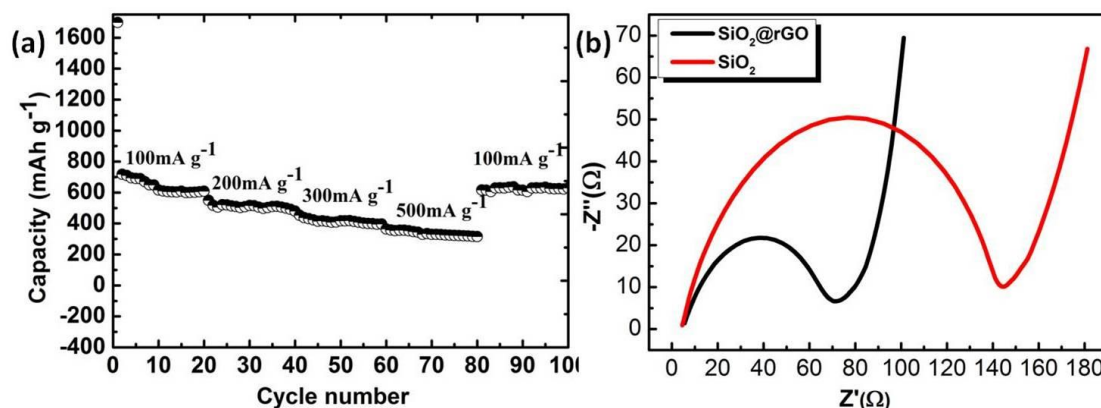


**Figure 5.** (a) rate performance of the SiO<sub>2</sub>@rGO nanocomposites; (b) EIS curves of nano-SiO<sub>2</sub> and SiO<sub>2</sub>@rGO nanocomposites.

It is showed that the resistance of the nano-SiO<sub>2</sub> electrode is almost twice as much as that of SiO<sub>2</sub>@rGO electrode comparing the diameter of the suppressed semicircle in high-medium frequency range. Thirdly, the superior structure flexibility and mechanic strength of rGO could deform resiliently to alleviate the fracture or pulverization of SiO<sub>2</sub> due to the volume changes upon repeated lithium insertion/extraction.

#### 4. CONCLUSIONS

In summary, the SiO<sub>2</sub>@rGO nanocomposites were fabricated successfully by a facile and scalable method for enhancing lithium ion storage of SiO<sub>2</sub> as high performance LIBs anode materials. Compared to nano-SiO<sub>2</sub>, the SiO<sub>2</sub>@rGO nanocomposites exhibit a higher reversible specific discharge capacity, excellent cycling stability and better rate capability for lithium ion storage. Such enhanced lithium storage performance of SiO<sub>2</sub>@rGO nanocomposites can result from its unique architecture features generating short lithium ions diffusion and electron transportation paths, excellent elasticity to accommodate the volume variation during repeated lithium charge-discharge process.

#### ACKNOWLEDGEMENTS

This work was supported by the Hubei Provincial Natural Science Foundation of China (No. 2015CFC842) and by the Education Science Foundation of Hubei Province (No. T200908).

#### References

1. J. Wang, H. Zhao, J. He, C. Wang and J. Wang, *J. Power Sources*, 196 (2011) 4811.
2. C. K. Chan, H. Peng, G. Liu, K. McIlwrath, X. F. Zhang, R. A. Huggins and Y. Cui, *Nat. Nanotechnol.*, 3 (2008) 31.
3. C. M. Park, J. H. Kim, H. Kim and H.-J. Sohn, *Chem. Soc. Rev.*, 39 (2010) 3115.

4. H. Wu, G. Chan, J.W. Choi, I. Ryu, Y. Yao, M.T. McDowell, S.W. Lee, A. Jackson, Y. Yang, L. Hu and Y. Cui, *Nat. Nanotechnol.*, 7 (2012) 309.
5. A. Magasinski, P. Dixon, B. Hertzberg, A. Kvit, J. Ayala and G. Yushin, *Nat. Mater.*, 9 (2010) 353.
6. M. N. Obrovac and L. Christensen, *Electrochem. Solid State Lett.*, 7 (2004) A93.
7. Y. Yao, M. T. McDowell, I. Ryu, H. Wu, N. Liu, L. Hu, W. D. Nix and Y. Cui, *Nano Lett.*, 11 (2011) 2949.
8. M. H. Park, M.G. Kim, J. Joo, K. Kim, J. Kim, S. Ahn, Y. Cui and J. Cho, *Nano Lett.*, 9 (2009) 3844.
9. L. Su, Z. Zhou and M. Ren, *Chem. Commun.*, 46 (2010) 2590.
10. Y. S. Hu, R. Demir-Cakan, M. M. Titirici, J. O. Mueller, R. Schloegl, M. Antonietti and J. Maier, *Angew. Chemie Int. Ed.*, 47 (2008) 1645.
11. F. Dai, R. Yi, M. L. Gordin, S. Chen and D. Wang, *RSC Adv.* 2 (2012) 12710.
12. H. Tao, L. Z. Fan, W. L. Song, M. Wu, X. He and X. Qu, *Nanoscale*, 6 (2014) 3138.
13. Y. Hwa, C. M. Park and H. J. Sohn, *J. Power Sources*, 222 (2013) 129.
14. N. Yan, F. Wang, H. Zhong, Y. Li, Y. Wang, L. Hu and Q. Chen, *Sci. Rep.*, 3 (2013) 32.
15. Z. Favors, W. Wang, H. H. Bay, A. George, M. Ozkan and C. S. Ozkan, *Sci. Rep.*, 4 (2014) 15.
16. N. Cao Cuong, H. Choi and S. W. Song, *J. Electrochem. Soc.*, 160 (2013) A906.
17. P. Lv, H. Zhao, J. Wang, X. Liu, T. Zhang and Q. Xia, *J. Power Sources*, 237 (2013) 291.
18. B. Gao, S. Sinha, L. Fleming and O. Zhou, *Adv. Mater.*, 13 (2001) 816.
19. W. S. Chang, C. M. Park, J. H. Kim, Y. U. Kim, G. Jeong and H. J. Sohn, *Energy Environ. Sci.*, 5 (2012) 6895.
20. L. Ji, Z. Lin, A. J. Medford and X. Zhang, *Carbon*, 47 (2009) 3346.
21. Q. Sun, B. Zhang and Z.-W. Fu, *Appl. Surf. Sci.*, 254 (2008) 3774.
22. S. Sim, P. Oh, S. Park and J. Cho, *Adv. Mater.*, 25 (2013) 4498.
23. J. Tu, Y. Yuan, P. Zhan, H. Jiao, X. Wang, H. Zhu and S. Jiao, *J. Phys. Chem. C*, 118 (2014) 7357.
24. B. Guo, J. Shu, Z. Wang, H. Yang, L. Shi, Y. Liu and L. Chen, *Electrochem. Commun.*, 10 (2008) 1876.
25. X. Cao, X. Chuan, S. Li, D. Huang and G. Cao, *Part. Part. Syst. Charact.*, 33 (2016) 110.
26. P. Lv, H. Zhao, J. Wang, X. Liu, T. Zhang and Q. Xia, *J. Power Sources*, 237 (2013) 291.
27. H. Xu, S. Zhang, W. He, X. Zhang, G. Yang, J. Zhang, X. Shi and L. Wang, *RSC Adv.*, 6 (2016) 1930.
28. Y. Yao, J. Zhang, L. Xue, T. Huang and A. Yu, *J. Power Sources*, 196 (2011) 10240.
29. X. Bai, Y. Yu, H.H. Kung, B. Wang and J. Jiang, *J. Power Sources*, 306 (2016) 42.
30. J. Meng, Y. Cao, Y. Suo, Y. Liu, J. Zhang and X. Zheng, *Electrochim. Acta*, 176 (2015) 1001.
31. Y. Yuan, S. Wang, Z. Kang and S. Jiao, *Electrochemistry*, 83 (2015) 421.
32. Y. Wang, W. Zhou, L. Zhang, G. Song and S. Cheng, *RSC Adv.*, 5 (2015) 63012.
33. H. Wang, P. Wu, M. Qu, L. Si, Y. Tang, Y. Zhou and T. Lu, *ChemElectroChem*, 2 (2014) 508.
34. W. S. Hummers and R. E. Offeman, *J. Am. Chem. Soc.*, 80 (1958) 1339.
35. J. Y. Luo, L. J. Cote, V. C. Tung, A. T. L. Tan, P. E. Goins, J. S. Wu and J. X. Huang, *J. Am. Chem. Soc.*, 132 (2010) 17667.
36. M. Srivastava, M. Elias Uddin, J. Singh, N. H. Kim and J. H. Lee, *J. Alloys Compd.*, 590 (2014) 266.
37. I. K. Moon, J. Lee, R. S. Ruoff and H. Lee, *Nat. Commun.*, 1 (2010) 73